PAPER

Check for updates

Increasing the thermal conductivity of styrene butadiene rubber: insights from molecular dynamics simulation

Xiuying Zhao,[abc] Bozhi Fu,[abc] Wenfeng Zhang,[abc] Haoxiang Li,[abc] Yonglai Lu,[abc] Yangyang Gao [ID] *[abc] and Liqun Zhang [ID] *[abc]

It is very important to improve the thermal conductivity of styrene butadiene rubber (SBR) which can widen its application. By employing reverse nonequilibrium molecular dynamics simulations in a full atomistic resolution, the effect of the composition ratio of styrene, temperature, and tensile strain on the thermal conductivity of SBR has been investigated in this work. The results indicate that the thermal conductivity of SBR gradually decreases with increasing composition ratio of styrene. This closely depends on the number of degrees of freedom and the diffusion coefficient of backbone atoms. Under the tensile field, the orientation of backbone bonds improves the thermal conductivity parallel to the tensile direction, but reduces the thermal conductivity perpendicular to it. Meanwhile, the thermal conductivity parallel to the tensile direction is enhanced with the strain rate while it is reduced with the composition ratio of styrene. Interestingly, there exists a linear relationship between the logarithm of anisotropy of the thermal conductivity and the orientation degree of bonds. Finally, the parallel thermal conductivity of the strained SBR first rises and then declines with temperature. This transition reflects a crossover from disorder to anharmonicity dominated phonon transport. Moreover, the transition temperature is gradually reduced with increasing strain which is attributed to the polymer orientation. In summary, this work provides some fundamental insights into the thermal transport processes in SBR with different composition ratios of styrene and temperature, especially under tensile strain.

1. Introduction

Fundamentally understanding thermal transport in polymers is essential for tuning thermal conductivity and accelerating their various applications such as thermal management and energy conversion.[1,2] In general, polymer materials have a very low thermal conductivity of 0.1–0.5 W m^{-1} K^{-1} at room temperature due to phonon scattering from numerous defects.[3] Even though engineering the thermal conductivity of polymer materials is of great technical importance, it remains a big challenge until now.

It is reported that the weak couplings between the polymer chains and their random orientation are two main reasons accounting for their low thermal conductivity.[4] Thus, various methods have been proposed and tried to enhance the thermal transfer in polymer materials. One method is to add the highly

[a]Key Laboratory of Beijing City on Preparation and Processing of Novel Polymer Materials, Beijing University of Chemical Technology, 10029, China. E-mail: gaoyy@mail.buct.edu.cn; zhanglq@mail.buct.edu.cn

[b]State Key Laboratory of Organic-Inorganic Composites, Beijing University of Chemical Technology, 100029, People's Republic of China

[c]Key Laboratory of Carbon Fiber and Functional Polymers, Ministry of Education, Beijing University of Chemical Technology, Beijing 100029, China

thermal conductive fillers into the polymers to improve their thermal conductivity.[5,6] However, this enhancement for the thermal transport is always inhibited because of the interfacial thermal resistance and the bad dispersion of fillers. The structure of polymer chains could also play an important role in the thermal conductivity. Generally, the stiff polymers with double –C=C– bonds and the conjugated π-bond on the backbone result in a higher thermal conductivity due to their high bonding energy.[7,8] Meanwhile, the thermal transport through covalent bonds is found to dominate the thermal conductivity than other contributions from the non-bonding interactions and the translation of molecules.[9] In addition, the thermal conductivity of polymer is found to decrease when side-chains are introduced which results from the phonon localization and phonon scatterings.[10,11] Interestingly, side-chains could also enhance the thermal conductivity of conjugated polymers due to the increase of their structural order.[12,13] Furthermore, enhancing inter-chain coupling strength could potentially produce a higher thermal conductivity of polymers. The thermal conductivity of polymer salts (poly(vinylsulfonic acid Ca salt)) is reported to be 0.67 W m^{-1} K^{-1} due to the relative strong electrostatic forces between the ions in different polymer chains.[14] Hydrogen bond is a strong electrostatic interaction between the proton and the lone electron pair(s) in O, N and F atom.[15–17] The

improvement of thermal conductivity is mainly attributed to the hydrogen bond which can help to form continuous thermal networks to provide more heat-transfer pathways. Similarly, crosslinks can form efficient thermal conduction pathways and networks by connecting polymer chains with covalent bonds which improves the thermal conductivity.[18,19] Moreover, the dependence of thermal conductivity of polyethylene (PE) on the temperature has been investigated which exhibits a consistent trend with the radius of gyration of chains.[20] Meanwhile, random orientation of the polymer chains can shorten the mean-free path of the phonons, which are the major energy carriers in polymers. Thus, another effective method to improve the thermal conductivity is to stretch the polymers which can enhance the order of chain orientation. For example, the thermal conductivity of the ultrahigh molecular weight PE can exceed 40 W m^{-1} K^{-1} when the drawing ratio is beyond 300.[21] Shen et al.[22] obtained a higher drawing ratio (400) and produced a PE nanofiber with a higher thermal conductivity of 104 W m^{-1} K^{-1}. In addition, the thermal conductivity of the electro-spinning polystyrene (PS) nanofibers is found to be between 6.6 and 14.4 W m^{-1} K^{-1} which is much larger than that (∼0.15 W m^{-1} K^{-1}) of bulk PS due to their preferential alignment.[23] The enhancement of thermal conductivity of polymers has also been observed by molecular dynamics simulation which is related to the polymer alignment.[24,25]

Based on the above works, although a large amount of research works has been devoted to enhance the thermal conductivity of polymers, a fundamental understanding of the inner mechanism has not been clearly identified yet. Especially, there is few works on the styrene butadiene rubber (SBR) which is an important component of tire tread in academic and industrial studies.[26,27] Thus, in this work, we employed the molecular dynamics simulations to study the effect of the composition ratio of styrene, temperature and tensile strain on the thermal conductivity of SBR which has not been investigated to our knowledge. By calculating the thermal conductivity, degrees of freedom of backbone atoms, and the orientation degree of backbone bonds, their inner relationship are revealed. Meanwhile, the effect of tensile strains on the transition temperature of the maximum thermal conductivity is discussed. The results can help to provide some fundamental insights into the thermal transport processes in the SBR.

2. Model and simulation methods

In this work, the adopted butadiene styrene rubber (SBR) is the random copolymers of the butadiene and the styrene. It is noted that the density of SBR basically doses not change when the number of their repeat units exceeds 50. Thus, a single chain contains 50 repeat units in the SBR model. The total number of chains is 30 which are identical for each system. There are four kinds of repeat units in one SBR chain which are the styrene, cis-1,4 butadiene, trans-1,4 butadiene and 1,2 butadiene respectively. Their composition ratio is listed in Table 1 for different systems. It is noted that the tacticity of styrene regions within the chains is atactic in our simulation.

Table 1 The details of the composition ratio of the styrene, cis-1,4 butadiene, trans-1,4 butadiene and 1,2 butadiene in one chain for different systems

Systems	Styrene (%)	cis-1,4 Butadiene (%)	trans-1,4 Butadiene (%)	1,2 Butadiene (%)
1	0	18	65	17
2	13	15.7	56.5	14.8
3	23	13.9	50	13.1
4	33	12.1	43.5	11.4
5	43	10.3	37	9.7
6	53	8.5	30.5	8.0
7	63	6.7	24	6.3
8	73	4.9	17.5	4.6
9	83	3.1	11	2.9
10	100	0	0	0

The condensed-phase optimized molecular potentials (COMPASS) are used to model the SBR which can accurately simulate the structural, vibrational, and thermo-physical properties of polymers.[28,29] Similar to our previous work,[30,31] all the SBR chains are put into a large simulation box to generate the initial configuration. Then, the isothermal–isobaric (NPT) ensemble is adopted to compress the system for 20 ns to reach the equilibrium density. The temperature and pressure are fixed at $T = 300$ K and $P = 101.3$ kPa respectively by using the Nose–Hoover temperature thermostat and pressure barostat respectively. Periodic boundary conditions are
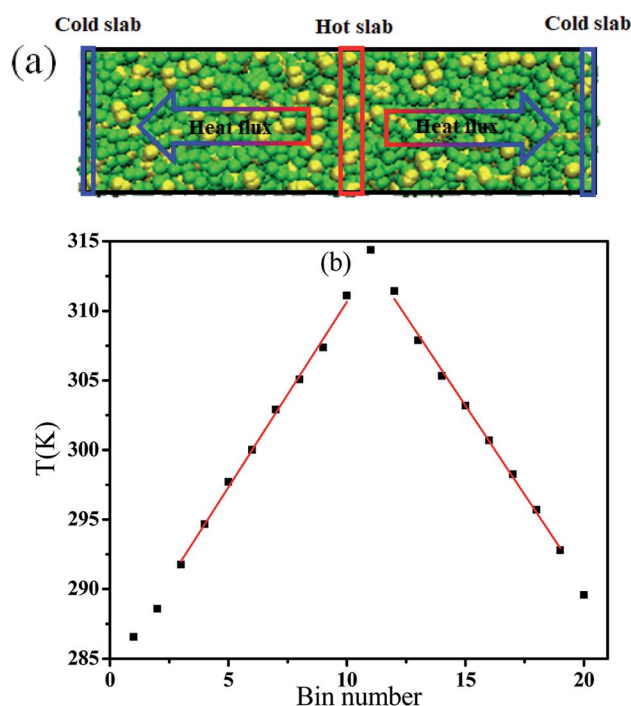
Fig. 1 (a) A snapshot of the deformed butadiene styrene rubber system and a NEMD setup to impose constant heat flux. (b) A stable linear temperature gradient obtained from NEMD simulation. ($T = 300$ K, strain = 2.0, composition ratio of styrene = 23%.)

employed in all three directions of the simulation box. The timestep for the leapfrog integration scheme is set to be 1.0 fs. Nonbonded interactions are calculated using a Verlet neighbor list, which is updated every 15 timesteps. Subsequently the obtained systems are further equilibrated at constant volume and temperature for 20 ns. The density is 0.89 g cm^{-3} and the glass transition temperature (the intersection point from the specific volume–temperature curve) is 238 K for the SBR which are in agreement with the measured data.[32] After equilibration, the simulation systems are deformed by changing the box length in one direction at a constant rate α. Meanwhile, the box length is reduced in the other two directions to keep the box volume unchanged during the deformation process. Three different tensile rates are considered here, namely 0.5 nm ns^{-1}, 5 nm ns^{-1}, and 50 nm ns^{-1}. A maximum strain of 300% is reached in this work. It is noted that there is no formation of voids or crazes for all systems. The average results are obtained by independently deforming each system along x, y and z directions, respectively.

Then, we adopted reverse nonequilibrium molecular dynamics (RNEMD) to calculate the thermal conductivity of the SBR.[33] In the RNEMD method, the velocity of the coldest atom in the first slab is exchanged with that of the hottest atom in the eleventh slab as a primary perturbation. During the simulation process, the total energy is conserved, because only velocities of atoms of identical mass are exchanged. In the calculation of the thermal conductivity, the simulation box is divided into 20 slabs in the heat flux direction. NVT conditions are adopted during the RNEMD process. The atom velocities are exchanged every 0.4 ps. We have confirmed that the calculated thermal conductivity has converged at this chosen exchange period. The trajectories are obtained for 5 ns, which are divided into ten independent blocks. Then we calculated the quantities separately in each block, determine average and standard deviation of the average, and use standard deviation as error bar. The thermal conductivity is calculated by using Fourier's law[33] $j_z =$
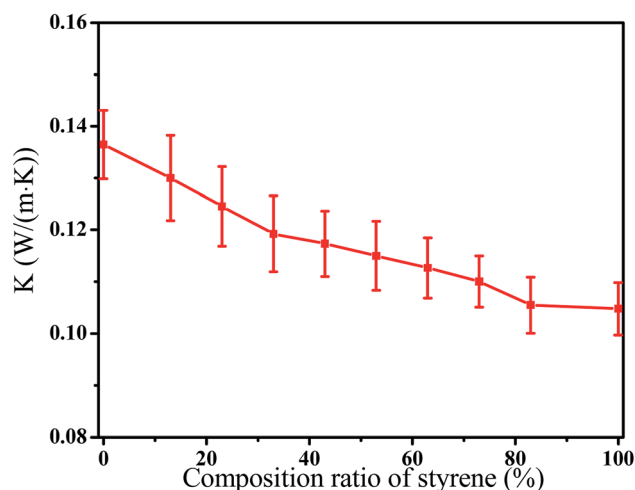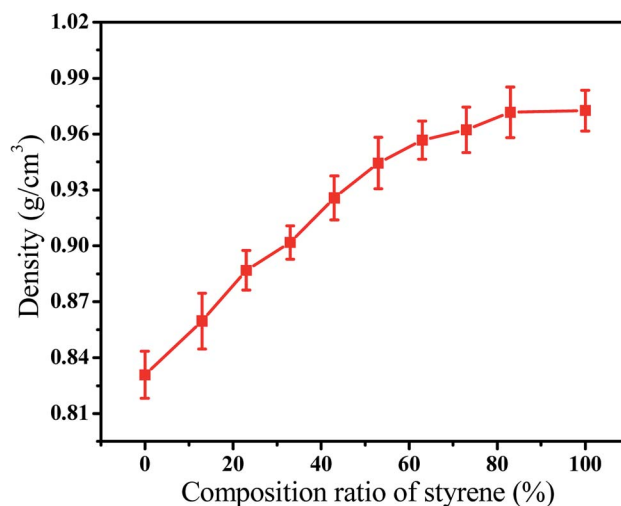
Fig. 3 The density of the butadiene styrene rubber as a function of the composition ratio of styrene. ($T = 300$ K, strain = 0.0.)
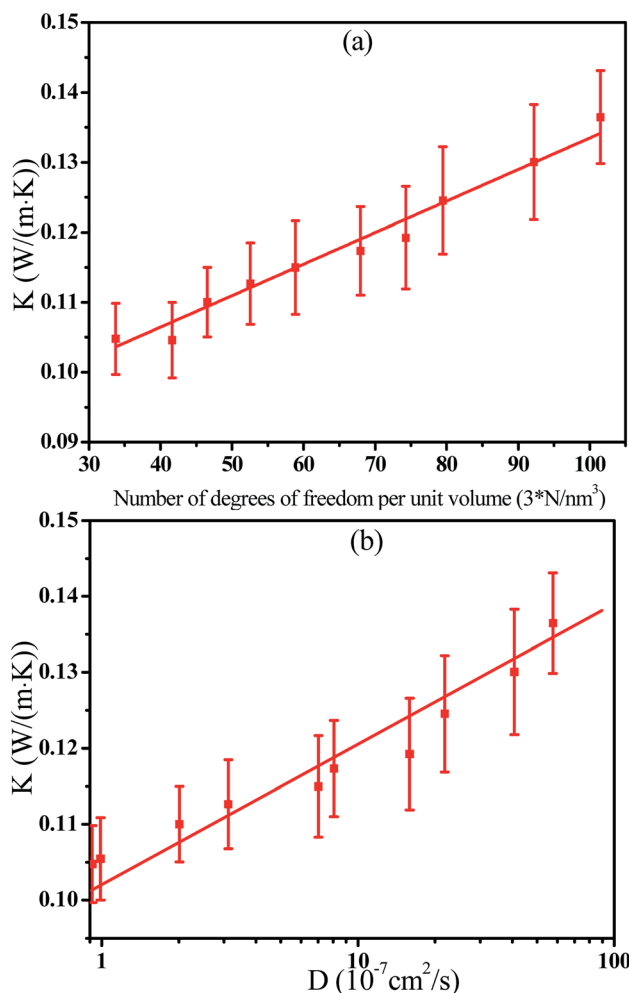
Fig. 4 The thermal conductivity K of the butadiene styrene rubber as a function of (a) the degrees of freedom of backbone atoms per unit volume and (b) the logarithm of diffusion coefficient (D) of backbone atoms. ($T = 300$ K, strain = 0.0.)

Fig. 2 The thermal conductivity K of the butadiene styrene rubber as a function of the composition ratio of styrene. ($T = 300$ K, strain = 0.0.)

$K\mathrm{d}T/\mathrm{d}z$. Here the j_z is the heat flux which is obtained by the equation $j_z = \dfrac{1}{2tA}\sum\limits_{\text{transfer}}\dfrac{m}{2}(v_{\text{hot}}^2 - v_{\text{cold}}^2)$, where m is the mass of the exchanged atoms, t is the simulation time, A is the cross-sectional area perpendicular to the heat flux, and v_{hot} and v_{cold} stand for the velocities of the hot and cold atoms of like mass m, respectively, whose velocities are exchanged. The factor 2 arises from the periodicity. $\mathrm{d}T/\mathrm{d}z$ is the stable temperature gradient in the intervening region which is shown in Fig. 1 as an example. The temperature T_{slab} within each slab is evaluated as

$$\frac{3N_{\text{slab}}k_{\text{B}}T_{\text{slab}}}{2} = \frac{1}{2}\left\langle \sum_{\substack{\text{atoms }i \\ \text{in slab}}}^{N} m_i v_i^2 \right\rangle$$ where the number of atoms in

the slab is N_{slab} and k_{B} is Boltzmann's constant. The angle brackets denote averaging over the atoms in the slab and over time. The sum is over all exchange events. It can refer to the previous work for a complete description of the RNEMD method.[34] All simulations have been performed by using the large scale atomic/molecular massively parallel simulator (LAMMPS).[35]

3. Results and discussion

3.1 Composition ratio of styrene

The composition ratio of styrene and butadiene in one chain can be tuned during the process of synthetizing the SBR according to their real application environment. Undoubtedly, it will affect the thermal conductivity of SBR. Thus, we first intended to investigate the effect of composition ratio of styrene on the thermal conductivity by fixing the repeat units. The composition ratio of styrene varies from 0% to 100% while the corresponding ratio of butadiene is from 100% to 0%. This is roughly within the experimental range.[32] Detailed information on the studied systems is shown in Table 1. The change of the thermal conductivity K of SBR with the composition ratio of styrene is presented in Fig. 2. The results indicate that the K gradually decreases with increasing the composition ratio of styrene. It is noted that when the composition ratio of styrene is 0% or 100%, the polymers are polybutadiene (PB) or polystyrene (PS). The simulated thermal conductivities are 0.135 W m^{-1} K^{-1} and $K = 0.105$ W m^{-1} K^{-1} for PB and PS respectively while the experimental values are 0.175 W m^{-1} K^{-1} and 0.11 W m^{-1} K^{-1}.[32] It is reported that the cross-linking density can enhance the thermal conductivity of PE which can explain the smaller K of PB in the simulation.[36] However, the very limited increase of thermal conductivity of PS with the cross-linking density is attributed to the highly heterogeneous PS structure including the phenyl side groups. Thus, the simulated and experimental K of PS are similar.[36] To further understand the results, the density of SBR is calculated as a function of the composition ratio of styrene which is shown in Fig. 3. The density decreases with an improved composition ratio of styrene which is attributed to the large phenyl side groups. It is noted that the number
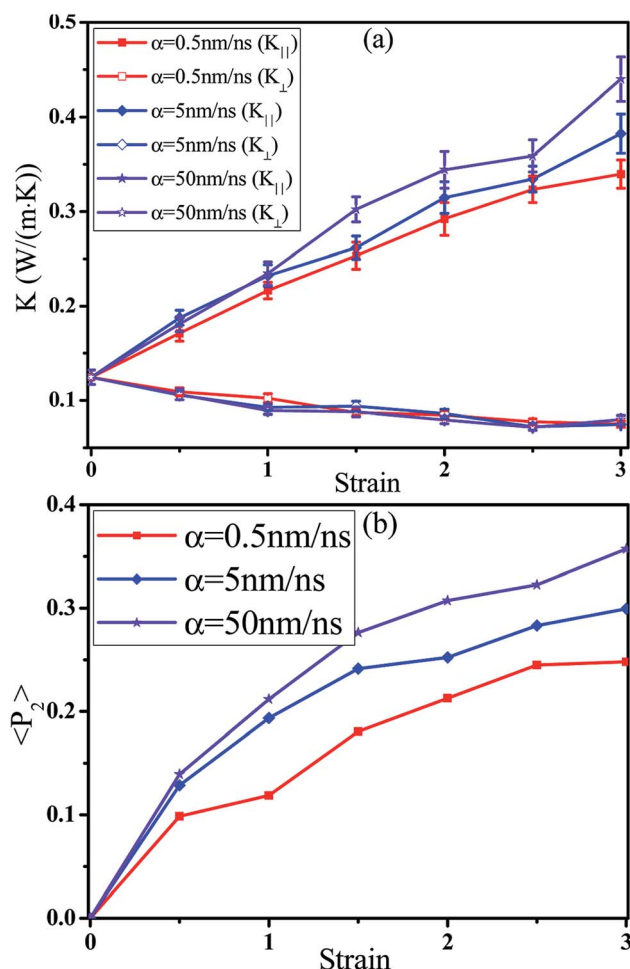

Fig. 5 Change of the thermal conductivities (a) $K_\parallel$ (W m^{-1} K^{-1}) parallel to tensile direction, $K_\perp$ (W m^{-1} K^{-1}) perpendicular to tensile direction, and (b) the orientation degree $\langle P_2 \rangle$ of backbone bonds with the strain for different tensile rates α. ($T = 300$ K, composition ratio of styrene = 23%.)
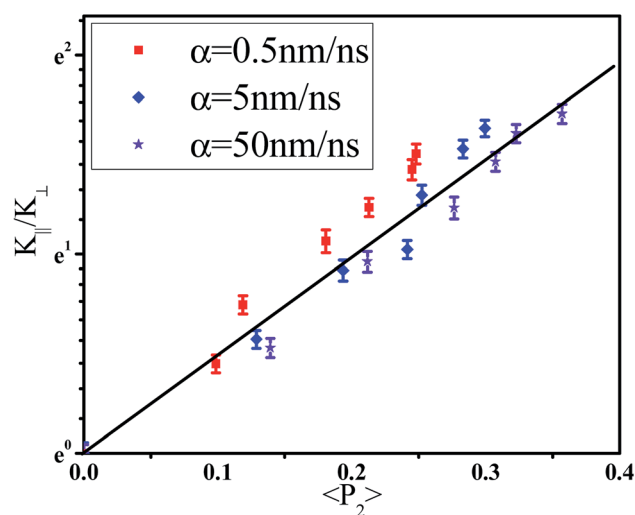

Fig. 6 Change of the logarithm of anisotropy of thermal conductivity $K_\parallel/K_\perp$ with the orientation degree $\langle P_2 \rangle$ of backbone bonds for different tensile rates α. ($T = 300$ K, composition ratio of styrene = 23%.)

of degrees of freedom of backbone atoms is one of decisive quantities for the thermal transport property. Here, it is defined as the $3 \times N$ where N is the number of backbone atoms in the system. Thus, we have calculated the thermal conductivity of SBR as a function of the number of degrees of freedom of backbone atoms per volume in Fig. 4(a). There is a linear correlation between them which can rationalize the thermal conductivity. As the increase of the composition ratio of styrene, the number of the backbone atoms is reduced at the fixed repeat unit which reduces the thermal conductivity. Furthermore, the dependence of the thermal conductivity on the logarithm of the diffusion coefficient of backbone atoms is presented in Fig. 4(b). It also exhibits a linear relationship between them which indicates that the high mobility of atoms can enhance the thermal conductivity.

3.2 Tensile field

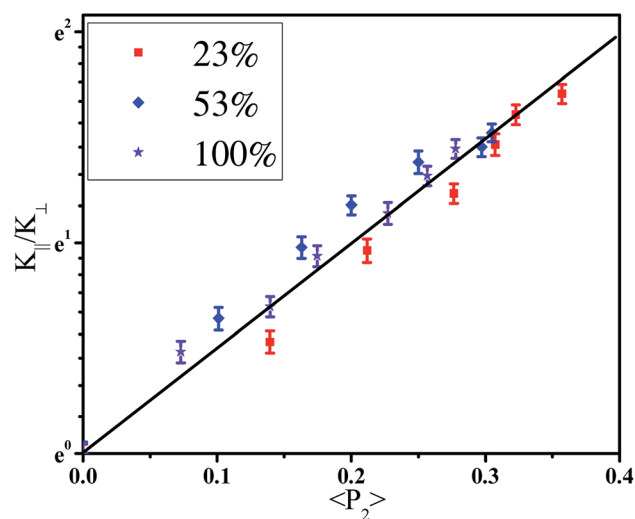**3.2.1 Tensile rate.** In general, the thermal energy transports more efficiently along the polymer chain (the strong

Fig. 8 Change of the logarithm of anisotropy of thermal conductivity $K_\parallel / K_\perp$ with the orientation degree $\langle P_2 \rangle$ of backbone bonds for different composition ratio of styrene. ($T = 300$ K, $\alpha = 50$ nm ns^{-1}.)
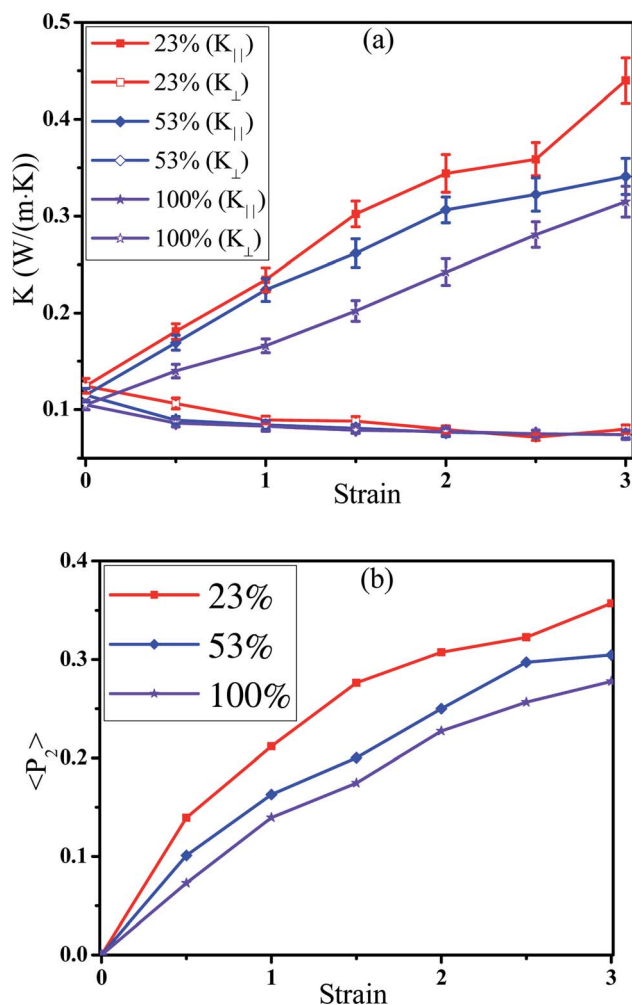

Fig. 7 Change of the thermal conductivities (a) $K_\parallel$ (W m^{-1} K^{-1}) parallel to tensile direction, $K_\perp$ (W m^{-1} K^{-1}) perpendicular to tensile direction, and (b) the orientation degree $\langle P_2 \rangle$ of backbone bonds with the strain for different composition ratio of styrene. ($T = 300$ K, $\alpha = 50$ nm ns^{-1}.)
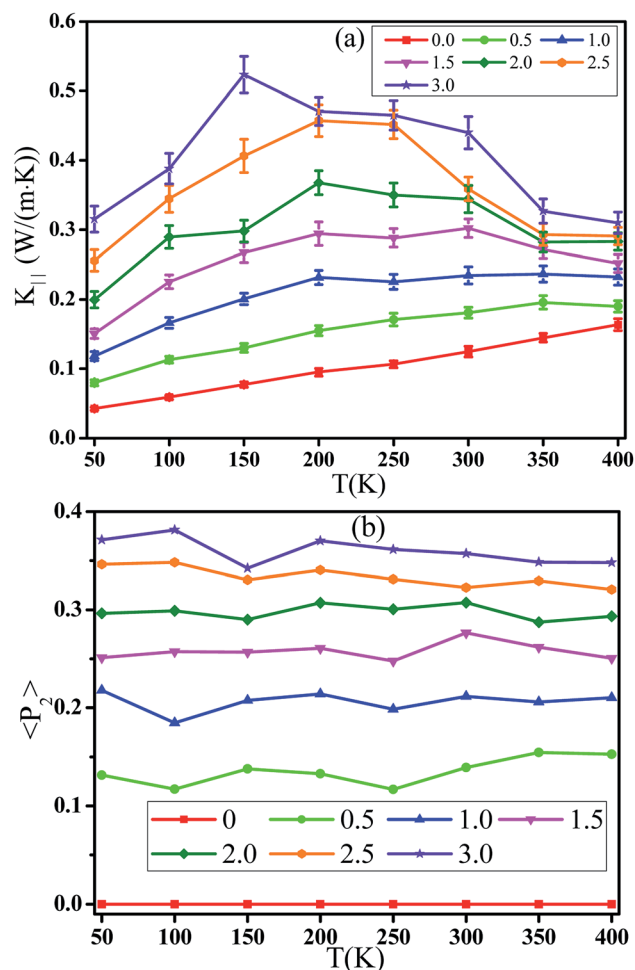

Fig. 9 Change of the (a) thermal conductivities $K_\parallel$ (W m^{-1} K^{-1}) parallel to tensile direction and (b) the orientation degree $\langle P_2 \rangle$ of backbone bonds with the temperature (T) for different strains. (Composition ratio of styrene = 23%, $\alpha = 50$ nm ns^{-1}.)
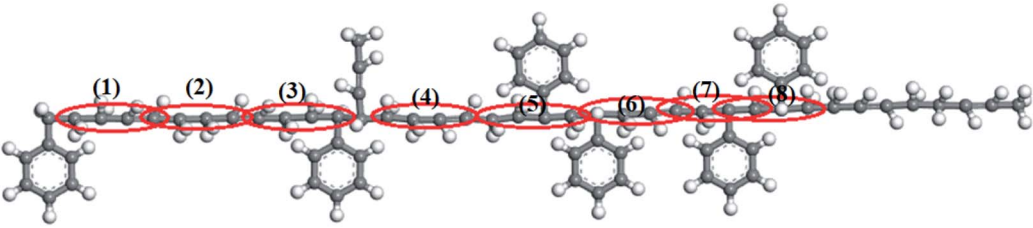
covalent bonds) than perpendicular to the polymer chain (van der Waals force). Thus, the tensile field can induce the orientation of backbone bonds along the tensile direction which can enhance the thermal conductivity.[24,37] Here, three different tensile rates α are considered here, namely 0.5 nm ns^{-1}, 5 nm ns^{-1}, and 50 nm ns^{-1}. The composition ratio of styrene is chosen to be 23% which stands for a common SBR. The thermal conductivities $K_\parallel$ parallel to the tensile direction and $K_\perp$ perpendicular to it are shown in Fig. 5(a) for different tensile rates α. $K_\parallel$ gradually increases while $K_\perp$ decreases with increasing the strain. Meanwhile, $K_\parallel$ shows an increase with the α while $K_\perp$ is nearly unchanged. Anisotropy of thermal conductivity $K_\parallel/K_\perp$ rises with the strain which is induced by the orientation of backbone bonds along the tensile direction. Here, the orientation degree of backbone bonds is defined by the second-order Legendre polynomials $\langle P_2 \rangle$. It is given by $\langle P_2 \rangle = (3\langle \cos^2 \theta \rangle - 1)/2$, where θ denotes the angle between the bond vector and the tensile direction. The parameter $\langle P_2 \rangle$ is 0.0 if the bonds are randomly oriented, 1.0 if the bonds are perfectly parallel to the tensile direction, and -0.5 if the bonds are perpendicular to it. Fig. 5(b) presents the orientation degree $\langle P_2 \rangle$ of backbone bonds with respect to the strain for different α. The $\langle P_2 \rangle$ is zero at strain = 0.0 which reflects the random orientation of bonds. Then, it shows a gradual increase with increasing the strain which reflects their orientation along the tensile direction. This is consistent with the thermal conductivity. To further understand their relationship, the dependence of the logarithm of $K_\parallel/K_\perp$ on the orientation degree $\langle P_2 \rangle$ of bonds is shown in Fig. 6. The results show a linear relationship between them ($\ln(K_\parallel/K_\perp) = 5.08\langle P_2 \rangle$), which indicates that the heat transfers mainly *via* the backbone bonds. In the previous work, Liu *et al.*[24] found that the relationship between the

parallel thermal conductivity of PE and the chain orientation follows an exponential equation. In addition, the anisotropy of the thermal conductivity $K_\parallel/K_\perp$ has a close relationship with the average direction cosine of the C–C backbone bonds for amorphous PS.[38] Furthermore, $K_\parallel$ increases by 37% while $K_\perp$ decreases by 12% at strain = 0.3 and $T = 300$ K for amorphous polyamide,[39] which means $K_\parallel/K_\perp \sim 1.5$. $K_\parallel$ increases by 8% while $K_\perp$ decreases by 11% at strain = 0.3 and $T = 400$ K for amorphous PS,[40] which means $K_\parallel/K_\perp \sim 1.2$. $K_\parallel/K_\perp$ varies from 1.91 to 1.05 for polyamide nanoconfined between graphene surfaces with the increase of the inter-surface width from 1 to 6 nm.[41] For our systems, $K_\parallel$ increases by 26%, $K_\perp$ decreases by 6.5%, and $K_\parallel/K_\perp$ is $\sim$1.35 at strain = 0.3 and $T = 300$ K. In total, our simulation results can be comparable to others.

3.2.2 Composition ratio of styrene. In Section 3.1, the thermal conductivity of SBR gradually decreases with increasing the composition ratio of styrene. Here, we intended to understand how the composition ratio of styrene influences the evolution of the thermal conductivity under the tensile field. The tensile rate α is 50 nm ns^{-1}. As shown in Fig. 7(a), the thermal conductivities $K_\parallel$ gradually decreases with the composition ratio of styrene at any strain while the $K_\perp$ is nearly unchanged. To explain it, the orientation degree $\langle P_2 \rangle$ of backbone bonds is calculated as a function of strain for different composition ratio of styrene in Fig. 7(b). It is found that the $\langle P_2 \rangle$ of backbone bonds gradually decreases with increasing the composition ratio of styrene. On one hand, the high composition ratio of styrene reduces the number of degrees of freedom of backbone atoms. Meanwhile, because of the large phenyl side groups, the conformational freedom of chains decreases. Such packing inhibits the reorientation of chains which leads to the low $\langle P_2 \rangle$. These results can

Table 2 The details of the original and modified parameters for dihedral angles on the backbone

Dihedral angle	Original parameters			Modified parameters		
	K_1 (kcal mol^{-1})	K_2 (kcal mol^{-1})	K_3 (kcal mol^{-1})	K_1 (kcal mol^{-1})	K_2 (kcal mol^{-1})	K_3 (kcal mol^{-1})
(1) C_4–C_4–$C_{3=}$–$C_{3=}$	0.243	0	0.104	−0.010	−0.200	−0.304
(2) $C_{3=}$–C_4–C_4–$C_{3=}$	0	0	−0.153	0.1500	0	−0.353
(3) $C_{3=}$–C_4–C_4–C_{43}	0	0	−0.153	0.1500	0	−0.353
(4) C_4–C_4–C_{43}–$C_{3=}$	0.088	0	−0.020	0.1000	0	−0.198
(5) C_4–C_4–C_{43}–C_4	0	0.051	−0.143	0	−0.100	−0.430
(6) C_{43}–C_4–$C_{3=}$–$C_{3=}$	0.243	0	0.104	0.2000	0	−0.2
(7) $C_{3=}$–C_4–C_{43}–C_4	0.088	0	−0.020	0.1	0	−0.198
(8) C_{43}–C_4–C_{43}–C_4	0	0.051	−0.143	0	0.514	−0.01

rationalize the observed thermal conductivity. Then, Fig. 8 presents the change of the anisotropy of the thermal conductivity $K_\parallel/K_\perp$ with the orientation degree $\langle P_2 \rangle$ of backbone bonds. Similarly, the logarithm of $K_\parallel/K_\perp$ exhibits a linear dependence on the $\langle P_2 \rangle$ which is $\ln(K_\parallel/K_\perp) = 5.01\langle P_2 \rangle$.

3.2.3 Temperature. Temperature is another important parameter which will affect the thermal conductivity of SBR. Here, the composition ratio of styrene is 23%. It is noted that the deformation process is performed at the corresponding temperature for all systems. The parallel thermal conductivity $K_\parallel$ at different strains and temperatures are provided in Fig. 9(a). A monotonic increase in $K_\parallel$ is observed with the strain at each temperature which has been explained above. Meanwhile, the $K_\parallel$ first increases and then decreases with the temperature for strain > 0.0. It is noted that the transition temperature at the maximum $K_\parallel$ is 450 K for strain = 0.0 (not shown). In addition, this transition temperature at the maximum $K_\parallel$ gradually decreases from 350 K to 150 K with the strain from 0.5 to 3.0. It is noted that the ratio of $K_\parallel$ (strain = 3.0) to $K_\parallel$ (strain = 0.0) gradually rises from 1.9 to 7.5 with reducing the temperature from 400 K to 50 K. This indicates that the enhanced amplitude of thermal conductivity is high at low temperatures. In other words, the strained SBR can be more effective for the thermal transfer at lower temperatures. Then, we calculated the orientation degree $\langle P_2 \rangle$ of backbone bonds at different strains and temperatures which are provided in Fig. 9(b). The $\langle P_2 \rangle$ is nearly independent of the temperature at any strain which can not explain the $K_\parallel$. The variation of the transition temperature with the strain can be understood by an interplay between disorder and anharmonic phonon scattering. It is reported that the thermal conductivity is calculated by $K \propto Cv^2\tau$,[42] where C, v, and τ are the specific heat, the group velocity and the lifetime of the phonon, respectively. The τ depends on the scattering rate because of both disorder and anharmonicity of polymer chains.[42] Disorder scattering involves the scattering of phonons from abrupt changes in the chain orientation and across polymer chains whose rates are nearly independent of the temperature.[43,44] However, the anharmonic scattering rates rise with increasing the temperature.[42] The disorder dominates the scattering mechanism because of the weak anharmonic effects at low temperature while the anharmonic scattering increases and begins to determine the phonon lifetimes at high temperature. It is observed that the disorder scattering is nearly unchanged at low temperature which leads to the constant τ. The specific heat C rises with increasing the temperature due to the anharmonic effect which enhances the thermal conductivity at low temperature.[45] The anharmonic scattering rates rise with the temperature at high temperature which reduces the τ. As a result, the thermal conductivity gradually decreases with the higher temperature. Thus, the thermal conductivity reaches the maximum value at the transition temperature which reflects a variation from disorder to anharmonicity dominated phonon transport. In our simulation, the high strain will shift the transition temperature to be a low value. First, the polymer chains have a large number of turns and bends which leads to the large disorder scattering rate at low strains.[46] Thus, a large anharmonic scattering rate is required to exceed the disorder

scattering rate which needs a high transition temperature. Then, the polymer chains are gradually aligned with increasing the strain which reduces the disorder scattering rate. Thus, a low transition temperature is enough to make the anharmonic scattering rate exceed the disorder scattering rate. These can rationalize the observed lower transition temperature with increasing the strain. It is noted that the dihedral energy parameters determine torsion angles which can tune the structure of the polymer chains. Meanwhile, the dihedral energies are much smaller than bond energies. Thus, the change of dihedral terms does not significantly impact vibrational frequencies which enable understanding the effect of change in disorder alone. As a result, the disorder is increased by changing the energy parameters of the C–C–C–C dihedral angles on the backbone which is the main relevant for determining the backbone structure. The details of the modified parameters for the dihedral angles on the backbone are listed in Table 2. For example, the energy profiles of the dihedral angle (5) are shown in Fig. 10(a) for the original and modified parameters. By reducing the energy corresponding to the
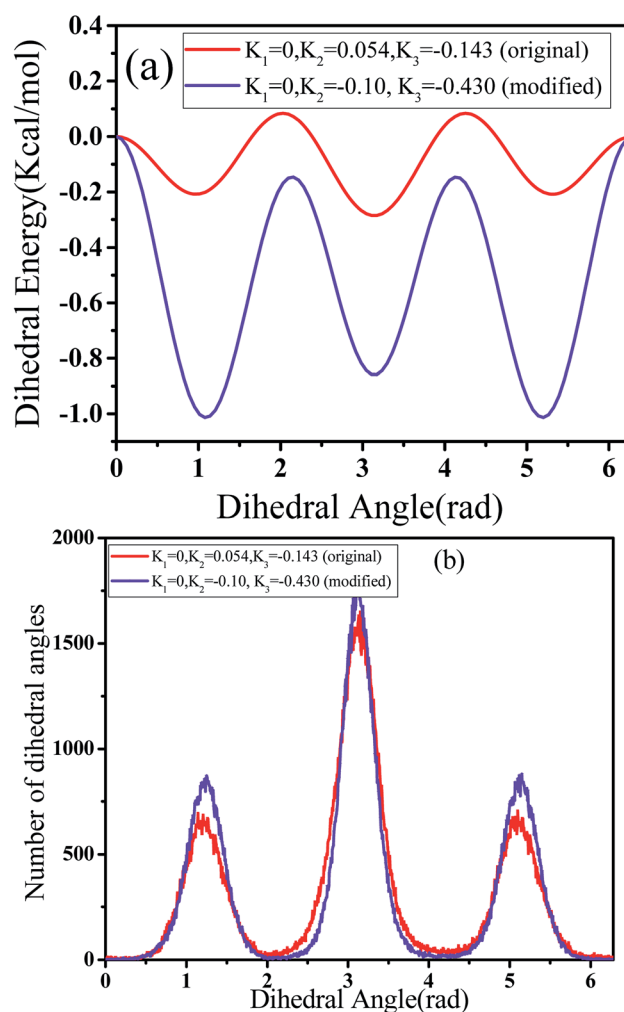

Fig. 10 (a) Dihedral energy and (b) number of dihedral angles for the original and modified dihedral parameters at strain = 3.0. (T = 300 K, composition ratio of styrene = 23%, α = 50 nm ns^{-1}.)
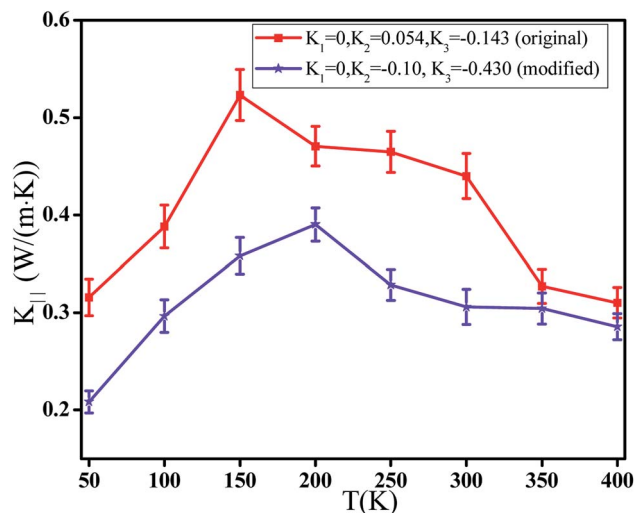
Fig. 11 Change of the thermal conductivities $K_{\parallel}$ ($W\ m^{-1}\ K^{-1}$) parallel to tensile direction with the temperature (T) for the original and modified dihedral parameters at strain = 3.0. (Composition ratio of styrene = 23%, $\alpha = 50\ nm\ ns^{-1}$.)

gauche state, the number of gauche configurations rises in Fig. 10(b). The thermal conductivity is calculated at strain = 3.0 for the system equilibration with a simulation at strain = 0 using the original and modified dihedral parameters. Then, the parallel thermal conductivity $K_{\parallel}$ is presented as a function of temperature at strain = 3.0 for the original and modified dihedral parameters in Fig. 11. The obtained $K_{\parallel}$ for the modified parameters is lower than that for the original parameters. This is because the change of the dihedral parameters leads to the higher disorder. Meanwhile, it increases the transition temperature at the maximum $K_{\parallel}$ from 150 K to 200 K. This can further prove the provided mechanism.

4. Conclusions

In the present work, we adopted reverse non-equilibrium molecular dynamics simulations in a full atomistic resolution to investigate the effect of the composition ratio of styrene, temperature and tensile strain on the thermal conductivity of styrene butadiene rubber (SBR). First, the number of backbone atoms declines with increasing the composition ratio of styrene which reduces their number of degrees of freedom and diffusion coefficient. Thus, the thermal conductivity of SBR exhibits a continuous decrease. The deformation induced polymer orientation enhances the thermal conductivity parallel to the tensile direction, but reduces the thermal conductivity perpendicular to it. Meanwhile, the orientation degree of backbone bonds gradually rises with increasing the strain rate or reducing the composition ratio of styrene which enhances the parallel thermal conductivity. It is interesting to observe a linear relationship between the anisotropy of the thermal conductivity and the orientation degree of backbone bonds. Finally, the thermal conductivity of the strained SBR first increases and then decreases with increasing the temperature

in the simulation. This can be explained by the transition from disorder to anharmonicity dominated phonon transport. Additionally, the high strain reduces the transition temperature which is attributed to the polymer orientation. Finally, it deserves to do the corresponding experimental investigations to prove it in the future. In summary, the obtained results are important to help to design the SBR for improving their thermal conductivity.

Conflicts of interest

There are no conflicts to declare.

Acknowledgements

References

1 M. A. Vadivelu, C. R. Kumar and G. M. Joshi, *Compos. Interfaces*, 2016, **23**, 847–872.
2 C. Huang, X. Qian and R. Yang, *Mater. Sci. Eng., R*, 2018, **132**, 1–22.
3 Z. Han and A. Fina, *Prog. Polym. Sci.*, 2011, **36**, 914–944.
4 J. Hennig, *J. Polym. Sci., Part C: Polym. Symp.*, 1967, **16**, 2751–2761.
5 R. Haggenmueller, C. Guthy, J. R. Lukes, J. E. Fischer and K. I. Winey, *Macromolecules*, 2007, **40**, 2417–2421.
6 A. Yu, P. Ramesh, M. E. Itkis, E. Bekyarova and R. C. Haddon, *J. Phys. Chem. C*, 2007, **111**, 7565–7569.
7 J. Liu and R. Yang, *Phys. Rev. B*, 2012, **86**, 104307.
8 Y. Xu, X. Wang, J. Zhou, B. Song, Z. Jiang, E. M. Y. Lee, S. Huberman, K. K. Gleason and G. Chen, *Sci. Adv.*, 2018, **4**, eaar3031.
9 V. Rashidi, E. J. Coyle, K. Sebeck, J. Kieffer and K. P. Pipe, *J. Phys. Chem. B*, 2017, **121**, 4600–4609.
10 H. Ma and Z. Tian, *Appl. Phys. Lett.*, 2017, **110**, 091903.
11 D. Luo, C. Huang and Z. Huang, *J. Heat Transfer*, 2018, **140**, 031302.
12 Z. Guo, D. Lee, Y. Liu, F. Sun, A. Sliwinski, H. Gao, P. C. Burns, L. Huang and T. Luo, *Phys. Chem. Chem. Phys.*, 2014, **16**, 7764–7771.
13 X. P. Chen, Q. H. Liang, J. K. Jiang, C. K. Y. Wong, S. Y. Y. Leung, H. Y. Ye, D. G. Yang and T. L. Ren, *Sci. Rep.*, 2016, **6**, 20621.
14 X. Xie, K. Yang, D. Li, T.-H. Tsai, J. Shin, P. V. Braun and D. G. Cahill, *Phys. Rev. B*, 2017, **95**, 035406.
15 X. Wei, T. Zhang and T. Luo, *Phys. Chem. Chem. Phys.*, 2016, **18**, 32146–32154.
16 G. H. Kim, D. Lee, A. Shanker, L. Shao, M. S. Kwon, D. Gidley, J. Kim and K. P. Pipe, *Nat. Mater.*, 2015, **14**, 295–300.
17 L. Mu, J. He, Y. Li, T. Ji, N. Mehra, Y. Shi and J. Zhu, *J. Phys. Chem. C*, 2017, **121**, 14204–14212.

18 B. Tonpheng, J. Yu and O. Andersson, *Phys. Chem. Chem. Phys.*, 2011, **13**, 15047–15054.

19 X. Xiong, M. Yang, C. Liu, X. Li and D. Tang, *J. Appl. Phys.*, 2017, **122**, 035104.

20 T. Zhang and T. Luo, *J. Phys. Chem. B*, 2016, **120**, 803–812.

21 C. L. Choy, Y. W. Wong, G. W. Yang and T. Kanamoto, *J. Polym. Sci., Part B: Polym. Phys.*, 1999, **37**, 3359–3367.

22 S. Shen, A. Henry, J. Tong, R. Zheng and G. Chen, *Nat. Nanotechnol.*, 2010, **5**, 251–255.

23 C. Canetta, S. Guo and A. Narayanaswamy, *Rev. Sci. Instrum.*, 2014, **85**, 104901.

24 J. Liu and R. Yang, *Phys. Rev. B*, 2010, **81**, 174122.

25 S. Pal, G. Balasubramanian and I. K. Puri, *J. Chem. Phys.*, 2012, **136**, 044901.

26 S. Song and Y. Zhang, *Carbon*, 2017, **123**, 158–167.

27 Z. Tang, L. Zhang, W. Feng, B. Guo, F. Liu and D. Jia, *Macromolecules*, 2014, **47**, 8663–8673.

28 H. Sun, *J. Phys. Chem. B*, 1998, **102**, 7338–7364.

29 M. J. McQuaid, H. Sun and D. Rigby, *J. Comput. Chem.*, 2004, **25**, 61–71.

30 Y. Gao and F. Müller-Plathe, *J. Phys. Chem. C*, 2018, **122**, 1412–1421.

31 Y. Gao and F. Müller-Plathe, *J. Phys. Chem. B*, 2016, **120**, 1336–1346.

32 J. E. Mark, *Polymer Data Handbook*, Oxford University Press, Oxford, 1999.

33 F. Müller-Plathe, *J. Chem. Phys.*, 1997, **106**, 6082–6085.

34 M. Zhang, E. Lussetti, L. E. S. de Souza and F. Müller-Plathe, *J. Phys. Chem. B*, 2005, **109**, 15060–15067.

35 S. Plimpton, *J. Comput. Phys.*, 1995, **117**, 1–19.

36 G. Kikugawa, T. G. Desai, P. Keblinski and T. Ohara, *J. Appl. Phys.*, 2013, **114**, 034302.

37 J. G. Park, Q. Cheng, J. Lu, J. Bao, S. Li, Y. Tian, Z. Liang, C. Zhang and B. Wang, *Carbon*, 2012, **50**, 2083–2090.

38 E. A. Algaer, M. Alaghemandi, M. C. Böhm and F. Müller-Plathe, *J. Phys. Chem. B*, 2009, **113**, 14596–14603.

39 E. Lussetti, T. Terao and F. Müller-Plathe, *J. Phys. Chem. B*, 2007, **111**, 11516–11523.

40 E. A. Algaer and F. Müller-Plathe, *Soft Mater.*, 2012, **10**, 42–80.

41 H. Eslami, L. Mohammadzadeh and N. Mehdipour, *J. Chem. Phys.*, 2012, **136**, 104901.

42 G. P. Srivastava, *The Physics of Phonons*, Taylor and Francis Group, New York, 1990, p. 418.

43 K. Eiermann, *J. Polym. Sci., Part C: Polym. Symp.*, 1964, **6**, 157–165.

44 J. Hennig, *J. Polym. Sci., Part C: Polym. Symp.*, 1967, **16**, 2751–2761.

45 S. N. Kreitmeier, G. L. Liang, D. W. Noid and B. G. Sumpter, *J. Therm. Anal.*, 1996, **46**, 853–869.

46 W. N. dos Santos, J. A. de Sousa and R. Gregorio, *Polym. Test.*, 2013, **32**, 987–994.